Sedimentation Analysis of Noninteracting and Self-Associating Solutes Using Numerical Solutions to the Lamm Equation

Peter Schuck

Molecular Interactions Resource, Bioengineering and Physical Science Program, OD, National Institutes of Health, Bethesda, Maryland 20892 USA

ABSTRACT   The potential of using the Lamm equation in the analysis of hydrodynamic shape and gross conformation of proteins and reversibly formed protein complexes from analytical ultracentrifugation data was investigated. An efficient numerical solution of the Lamm equation for noninteracting and rapidly self-associating proteins by using combined finite-element and moving grid techniques is described. It has been implemented for noninteracting solutes and monomer-dimer and monomer-trimer equilibria. To predict its utility, the error surface of a nonlinear regression of simulated sedimentation profiles was explored. Error contour maps were calculated for conventional independent and global analyses of experiments with noninteracting solutes and with monomer-dimer systems at different solution column heights, loading concentrations, and centrifugal fields. It was found that the rotor speed is the major determinant for the shape of the error surface, and that global analysis of different experiments can allow substantially improved characterization of the solutes. We suggest that the global analysis of the approach to equilibrium in a short-column sedimentation equilibrium experiment followed by a high-speed short-column sedimentation velocity experiment can result in sedimentation and diffusion coefficients of very high statistical accuracy. In addition, in the case of a protein in rapid monomer-dimer equilibrium, this configuration was found to reveal the most precise estimate of the association constant.

INTRODUCTION

Analytical ultracentrifugation is one of the traditional tools for the physical characterization of biological macromolecules. The concentration profiles of sedimenting macromolecules reveal, applying first principles, their molar masses, state of aggregation, diffusion coefficients, and hydrodynamic shapes. In particular, during the last decades, it has been used as a powerful technique for the characterization of homogeneous and heterogeneous protein-protein interactions and protein-nucleic acid interactions in solution. The traditional experimental configurations used are both high-speed long-column sedimentation velocity experiments, which observe the time course of the transient states, and low-speed sedimentation equilibrium experiments with shorter solution columns, in which the approached equilibrium between sedimentation and diffusion allows for the application of thermodynamic principles to the data analysis. Despite its success, in both configurations the information contained in the dynamics of the sedimentation process has not been exploited to its fullest potential, in particular with respect to hydrodynamic shape and gross conformation of reversibly formed protein complexes.

In 1929, Lamm derived the basic differential equation that governs the sedimentation behavior of ideal solutions, which has later been refined and generalized by Fujita (1962). For ideal solutions of chemically reacting solutes, it

takes the form

$$\frac{\partial c_k}{\partial t} + \frac{1}{r}\frac{\partial (rJ_{k,tr})}{\partial r} = Q_k$$

$$J_{k,tr} = \left[s_k\omega^2 r c_k - D_k\frac{\partial c_k}{\partial r} \right]$$

(1)

where $c_k(r, t)$ denotes the concentration of solute k at radius r and time t, $J_{k,tr}$ denotes the transport flux of solute k, ω denotes the angular velocity of the rotor, s_k and D_k denote the sedimentation and diffusion coefficients of the solute, and Q_k denotes the local chemical reaction rates, respectively (Fujita, 1962). In part because of the lack of analytical solutions, the data interpretation and the experimental techniques commonly had to be constrained to conditions that allow for analysis with special solutions to this equation. Sedimentation equilibrium can be understood as a special case of the Lamm equation, and others are the limit of negligible influence of diffusion on the sedimentation of noninteracting and self-associating solutes in high centrifugal fields (Fujita, 1962; Gilbert, 1955; Schachman, 1959; Svedberg and Pedersen, 1940), or the limit of an infinitely long solution column, which can be experimentally approached in high-speed experiments with larger macromolecules (Behlke and Ristau, 1997; Fujita, 1962; Holladay, 1979a; Philo, 1997; Stafford, 1992). While these special solutions have proven extremely useful, in practice they are not always completely satisfying. For example, difficulties can be encountered in the case of small, rapidly diffusing solutes (Schuck et al., 1998). Also, the traditional sedimentation velocity methods do not allow for completely rigorous data interpretation in the presence of chemical reactions.

Finally, they can restrict the experimenter in the choice of rotor speed, sample volume, and experiment time.

With the advent of digital computers, several investigators developed methods for numerical simulation of transport processes and demonstrated the principle of using numerical solutions of the Lamm equation for centrifugal data analysis (see, e.g., Bethune and Kegeles, 1961a, b; Cann and Kegeles, 1974; Claverie, 1976; Claverie et al., 1975; Cox, 1965, 1969; Dishon et al., 1966; Gilbert and Gilbert, 1973; Goad and Cann, 1969; Marque, 1992; Minton, 1992; Sartory et al., 1976). More recently, with increasing computational power readily at hand, increasing interest has been devoted to this approach. Based predominantly on the numerical methods described by Claverie and co-workers (1975), its potential for the description of experimental sedimentation data has been shown in different experimental configurations (Demeler and Saber, 1998; MacPhee et al., 1997; Schuck et al., 1998; Schuck and Millar, 1998; Stafford, 1998). In principle, numerical solutions allow the analysis of any series of concentration profiles, including those that previously have eluded quantitative analysis, e.g., the complete approach to equilibrium in low-speed experiments, and sedimentation velocity profiles that are governed by high diffusion and effects of the finite length of the solution column. This more direct numerical analysis has the potential for significant reduction of experimental time (Schuck and Millar, 1998) and reduction of sample volume, as well as an increase in the amount of data and the statistical accuracy of the results. Most importantly, these numerical approaches have the potential to rigorously take into account and obtain information about interacting systems of macromolecules, which is among the most useful and challenging of the current applications of analytical ultracentrifugation. Unfortunately, excessive computational cost still appears to limit the practicability of the extension of transient state analysis to interacting systems.

The present paper first describes an efficient finite element method for the numerical solution of the Lamm equation that extends the method described by Claverie et al. (1975) by the use of a moving grid. Second, the error surfaces of direct Lamm equation analyses are explored, and the use of a global analysis approach is proposed, which is already well-known to improve accuracy of results in sedimentation equilibrium analyses. Here, we demonstrate its advantages in the simultaneous analysis of sets of nonequilibrium data from experiments at different rotor speeds. Finally, an analytical procedure is described for solutes that exhibit homogeneous associations, in the ideal limit of instantaneous equilibria. It will be shown how both techniques of using a moving grid and a global analysis can be particularly helpful for the latter problem. All proposed methods have been implemented in a PC computer program running on the Windows operating system for the analysis of data from the Optima XL-A; this software is available on request.

METHODS

Moving grid

The central new aspect of the numerical method for obtaining solutions to the Lamm equations proposed in this paper is the incorporation of a moving frame of reference into a finite element approach. Similar to the change of radial variables used in the derivation of approximate analytical solutions to the Lamm equation (Faxén, 1929; Fujita and MacCosham, 1959; Fujita, 1962), the strategy here will be to transform the spatial coordinate such that the sedimentation term in the numerical solution of the Lamm equation disappears (Zienkiewicz and Taylor, 1991). This transformation of the grid will be described first in some detail.

The concentration distributions $c(r, t)$ are approximated by linear combinations of the elements $P_k(r, t)$

$$c(r, t) \approx \sum_{k=1}^{N} c_k(t) P_k(r, t) \tag{2}$$

They are hat functions (Fig. 1), defined as

$$P_k(r, t) = \begin{cases} (r - r_{k-1})/(r_k - r_{k-1}) & r_{k-1} \leq r \leq r_k \\ (r_{k+1} - r)/(r_{k+1} - r_k) & r_k < r \leq r_{k+1} \\ 0 & \text{else} \end{cases}$$

for $k = 2, \ldots, N - 1$, and

$$P_1(r, t) = \begin{cases} (r_2 - r)/(r_2 - r_1) & r_1 \leq r \leq r_2 \\ 0 & \text{else} \end{cases} \tag{3}$$

$$P_N(r, t) = \begin{cases} (r - r_{N-1})/(r_N - r_{N-1}) & r_{N-1} \leq r \leq r_N \\ 0 & \text{else} \end{cases},$$

where $r_k(t)$ denotes a division of the solution column in N (usually in the order of 1000) grid points lying between the meniscus and bottom. The hat functions $P_k(r, t)$ are similar to the elements used by Claverie and co-workers (1975), except for the nonequidistant and time-dependent grid $r_k(t)$ used in the present study. To enable the numerical separation of the effects
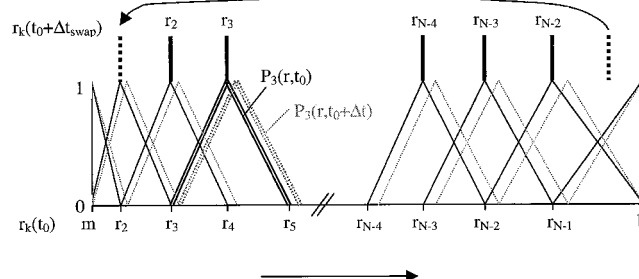

FIGURE 1   Schematic representation of the nonequidistant grid $r_k(t)$ and the corresponding elements $P_k(r, t)$. Solid lines indicate the hat functions $P_k(r, t_0)$ at the start of sedimentation; as an example, the hat function $P_3(r, t_0)$ is emphasized by double lines. At times $t_0 + \Delta t$ all grid points except $r_1 = m$ and $r_N = b$ move to larger radii, indicated by the broken lines. Spacing of the grid (Eq. 5) and the stretching in time (Eq. 4) is such that after the time Δt_{swap} (Eq. 6) the grid is mapped onto itself (Eq. 7). Grid positions at times t_0 and $t_0 + \Delta t_{swap}$ are indicated by solid vertical lines on the bottom and on top of the hat functions, respectively. At the time $t_0 + \Delta t_{swap}$, grid point $r_{N-1}(t_0 + \Delta t)$ (dotted line) is removed and inserted at $r_2(t_0)$.

of sedimentation and diffusion, the grid is moved according to

$$r_k(t) = r_{k,0}\alpha(t - t_0)$$

$$= r_{k,0}\exp\{s_G\omega^2(t - t_0)\} \quad \text{for} \quad k = 2, \ldots, N$$

$$r_1(t) = m, \quad r_N(t) = b, \tag{4}$$

where m and b denote the meniscus and bottom, respectively, of the solution column (Fig. 1). Except for the constant boundaries at $r_1 = m$ and $r_N = b$, this propagation $\alpha(t)$ describes that of an ideal sedimenting particle at $r_{k,0}$ with a sedimentation coefficient s_G and in the absence of diffusion. With the choice of the starting grid

$$r_{k,0} = m(b/m)^{(k-3/2)/(N-1)} \quad \text{for} \quad k = 2, \ldots, N - 1 \tag{5}$$

it follows that after a time interval of propagation

$$\Delta t_{\text{swap}} = [\omega^2 s_G(N - 1)]^{-1}\ln(b/m) \tag{6}$$

the grid is mapped precisely onto the starting grid

$$r_k(t_0 + \Delta t_{\text{swap}}) = r_{k+1,0} \quad \text{for} \quad k = 2, \ldots, N - 2 \tag{7}$$

This can be exploited to fall back on the starting grid $r_{k,0}$ in our description of $c(r, t)$, simply by incrementing all indices in c_k from 2 to $N - 2$ by one, and by adding Δt_{swap} to the reference time t_0 in Eq. 4. Additionally, the grid point at r_{N-1} is removed, and a new grid point $r_2 = r_{2,0}$ is inserted (Fig. 1). The concentration c_2 assigned to the new grid point r_2 is given by linear interpolation between m and r_3, whereas the effects of eliminating the grid point r_{N-1} can be taken into account by recalculating c_N, preserving total mass.

This definition of $r_k(t)$ retains a constant average density of points along the solution column. However, this grid constitutes a frame of reference that moves with the sedimenting solutes and therefore lends itself to description of sedimentation, particularly in the limit of small diffusion influence.

Solution of the Lamm equation in the absence of chemical reactions

In the following treatment, the absence of chemical reactions is assumed, i.e., $Q_k = 0$ in Eq. 1. With the approximation of Eq. 2, equations for the coefficients $c_k(t)$ can be derived by integrating the Lamm equation over the elements P_k

$$\int_m^b \frac{\partial c}{\partial t}P_k(r, t)rdr = -\int_m^b \frac{\partial(rJ)}{\partial r}P_k(r, t)rdr \tag{8}$$

and integration by parts of the rhs, exploiting the vanishing flux at the meniscus and bottom (Claverie et al., 1975), which leads to

$$\int_m^b \frac{\partial c}{\partial t}P_k(r, t)rdr = s\omega^2\int_m^b c\frac{\partial P_k(r, t)}{\partial r}r^2dr$$

$$- D\int_m^b \frac{\partial c}{\partial r}\frac{\partial P_k(r, t)}{\partial r}rdr \tag{9}$$

Insertion of Eq. 2 leads to a system of N equations for $c_j(t)$

$$0 = \sum_j \frac{\partial c_j}{\partial t}\int_m^b P_jP_krdr + \sum_j c_j\int_m^b \frac{\partial P_j}{\partial t}P_krdr$$

$$- \omega^2s\sum_j c_j\int_m^b P_j\frac{\partial P_k}{\partial r}r^2dr + D\sum_j c_j\int_m^b \frac{\partial P_j}{\partial r}\frac{\partial P_k}{\partial r}rdr$$

$$\tag{10}$$

The time derivative of the hat functions with $k = 3, \ldots, N - 2$ can be written as

$$\frac{\partial P_k}{\partial t} = \omega^2 s_G \times \begin{cases} -r/(r_k - r_{k-1}) & r_{k-1} \leq r \leq r_k \\ r/(r_{k+1} - r_k) & r_k < r \leq r_{k+1} \\ 0 & \text{else} \end{cases} \tag{11}$$

and similar expressions can be found for the elements 1, 2, $N - 1$, and N, taking into account that $r_1 = m$ and $r_N = b$ remain constant in time. Finally, we can transform Eq. 10 into the moving frame of reference using the change of variables $\rho(r, t) = r/\alpha(t - t_0)$, which allows us to separate the time-dependence $\alpha(t)$ out of the integrals. The results of the integrals are listed in the Appendix, expressed as tridiagonal matrices $\mathbf{B}$, $\mathbf{A}^{(1)}$, $\mathbf{A}^{(2)}$, and $\mathbf{A}^{(3)}$. Unfortunately, it is not possible to obtain time-independent expressions for those integrals involving hat functions P_1, P_2, P_{N-1}, and P_N, because in the moving frame of reference the position of meniscus $\rho(m)$ and bottom $\rho(b)$ will be time-dependent. Therefore, $\mathbf{B}(t)$, $\mathbf{A}^{(1)}(t)$, $\mathbf{A}^{(2)}(t)$, and $\mathbf{A}^{(3)}(t)$ are time-dependent only in the corner diagonal 2 × 2 submatrices due to the time-dependent transformations $\rho(m)$ and $\rho(b)$. This simplifies Eq. 10 to

$$\sum_j \frac{\partial c_j}{\partial t}\mathbf{B}_{kj}(t) = \sum_j\{\omega^2[s\mathbf{A}_{kj}^{(2)}(t) - s_G\mathbf{A}_{kj}^{(3)}(t)]$$

$$\tag{12}$$

$$- D\alpha^{-2}(t - t_0)\mathbf{A}_{kj}^{(1)}(t)\}c_j$$

This matrix equation is analogous to that derived by Claverie and co-workers using hat functions on a static and equidistant grid (see Eq. 11 in Claverie et al., 1975). However, it is generalized by a term $s_G\omega^2\mathbf{A}^{(3)}(t)$, that describes the movement of the frame of reference, and by the factor $\alpha^{-2}(t)$ that corrects the diffusion term for the stretching of the frame of reference.

It can be shown that $\mathbf{A}^{(2)} - \mathbf{A}^{(3)} = -2\mathbf{B}$ is true for all elements except those with $k, j = 1, 2, N - 1$, or N. Ignoring these elements would correspond to the common ideal assumption of an infinite solution column. In this limit, for $s_G = s$, the first term on the rhs coincides with the well-known expression for the radial dilution in the sector-shaped solution column, superimposed by the second term describing the diffusion. Sedimentation does not explicitly occur anymore in Eq. 12, it has been transformed into the movement of the grid. However, if $s_G = 0$ the grid remains static and the method approaches that reported previously (Claverie et al., 1975).

For the discretization of Eq. 12 in time, a Crank-Nicholson scheme (Crank and Nicholson, 1947) is useful in providing stability for larger time steps (Goad and Cann, 1969; Press et al., 1992). Evaluation of the time derivative on the lhs of Eq. 12 using the average of the rhs between time t and $t + \Delta t$ gives the matrix equation

$$[\mathbf{B}(t) + \mathbf{B}(t + \Delta t) - \Delta t\mathbf{J}(t + \Delta t)]\vec{c}(t + \Delta t)$$

$$= [\mathbf{B}(t) + \mathbf{B}(t + \Delta t) + \Delta t\mathbf{J}(t)]\vec{c}(t)$$

$$\mathbf{J}(t) = \omega^2[s\mathbf{A}_{kj}^{(2)}(t) - s_G\mathbf{A}_{kj}^{(3)}(t)] - D\alpha^{-2}(t - t_0)\mathbf{A}_{kj}^{(1)}(t) \tag{13}$$

(using the abbreviation $\vec{c}$ for the vector of concentrations c_k), which can be efficiently solved. Obviously, if the grid is moved with $s_G = s$ the time step Δt cannot exceed $3/2 \times \Delta t_{swap}$ without violating $r_{N-1} \leq b$. A particularly attractive choice for the time step is $\Delta t = \Delta t_{swap}$, for which each step with Eq. 13 is followed by incrementing the indices of concentrations. In accordance with the method of mapping the grid onto itself in time intervals Δt_{swap} (as outlined above, using Eq. 7), it follows that for each propagation step in Eq. 13 the matrices remain identical:

$$[\mathbf{B}^* - \Delta t \mathbf{J}_\Delta^*]\vec{c}(t + \Delta t_{swap}) = [\mathbf{B}^* + \Delta t \mathbf{J}^*]\vec{c}(t) \quad (14)$$

with $\mathbf{B}^* = \mathbf{B}(t_0) + \mathbf{B}(t_0 + \Delta t_{swap})$, $\mathbf{J}^* = \mathbf{J}(t_0)$, and $\mathbf{J}^*_\Delta = \mathbf{J}(t_0 + \Delta t_{swap})$. Therefore, they need to be calculated only once and the movement of the grid essentially does not increase the computational cost of the approach.

Solution of the Lamm equation in the limit of rapid self-associations

The simplest system of reacting solutes is that of monomers in rapid self-association equilibrium with oligomers. As outlined by Cox (1969), this case can be approximated by the introduction of locally concentration dependent weight-average sedimentation coefficients $s_w(c)$ and gradient-average diffusion coefficients $D_g(c)$:

$$s_w(c) = \sum_j K_j s^{(j)} c_1^{j-1} / \sum_j K_j c_1^{j-1}$$

$$D_g(c) = \sum_j j K_j D^{(j)} c_1^{j-1} / \sum_j j K_j c_1^{j-1} \quad (15)$$

where K_j denotes the association constant for the monomer-j-mer interaction (with $K_1 = 1$), c_1 denotes the monomer concentration, and $s^{(j)}$ and $D^{(j)}$ denote the sedimentation and diffusion coefficients of a j-mer, respectively. The monomer concentrations c_1 can be calculated locally from the total concentration c using the mass action law. With the approximation

$$s_w(r, t) \approx \sum_k s_w(c_k(t)) P_k(r, t) =: \sum_k s_{w,k}(c_k) P_k(r, t)$$

$$D_g(r, t) \approx \sum_k D_g(c_k(t)) P_k(r, t) =: \sum_k D_{g,k}(c_k) P_k(r, t) \quad (16)$$

we can extend the ideal single noninteracting solute calculations shown above. This follows a procedure similar to that described already by Claverie (1976) for the case of concentration-dependent sedimentation, here generalized to moving elements. The sedimentation coefficient of the grid was chosen to be the average of the monomer and oligomer sedimentation coefficients. Insertion into Eq. 9 leads to an extension of Eq. 10.

$$0 = \sum_j \frac{\partial c_j}{\partial t} \int_m^b P_j P_k r\, dr + \sum_j c_j \int_m^b \frac{\partial P_j}{\partial t} P_k r\, dr$$

$$- \omega^2 \sum_{j,i} c_j s_{w,i}(c_i) \int_m^b P_i P_j \frac{\partial P_k}{\partial r} r^2\, dr$$

$$+ \sum_{j,i} c_j D_{g,i}(c_i) \int_m^b P_i \frac{\partial P_j}{\partial r} \frac{\partial P_k}{\partial r} r\, dr \quad (17)$$

Again, the integrals over threefold products of hat functions evaluate to simple polynomials and can be abbreviated as tensors $\mathbf{U}_{kji}$ and $\mathbf{W}_{kji}$, which are non-zero only for $|k - j|, |k - i|, |j - i| < 2$ (see Appendix). Although they are time-dependent in their corner elements $k, j, i = 1, 2, N - 1$, or

N, again, they do not change for time steps Δt_{swap}. Generalization of the flux matrix $\mathbf{J}$ in Eq. 13 to

$$\mathbf{J}_{kj}(\vec{c}, t) = \omega^2 \left(-s_G \mathbf{A}_{kj}^{(3)}(t) + \sum_i s_{w,i}(c_i) \mathbf{U}_{kji}(t) \right)$$

$$- \alpha^{-2}(t - t_0) \sum_i D_{g,i}(c_i) \mathbf{W}_{kji}(t) \quad (18)$$

leads to an equation identical to Eq. 14. One additional complication of interacting systems is the concentration dependence of the fluxes, making Eq. 14 nonlinear. It can be addressed by using a two-step approximation

$$\vec{c}^{(pred)}(t + \Delta t) = \{\mathbf{B}^* - \Delta t \mathbf{J}_\Delta^*[\vec{c}(t)]\}^{-1}\{\mathbf{B}^* + \Delta t \mathbf{J}^*[\vec{c}(t)]\}\vec{c}(t)$$

$$\vec{c}(t + \Delta t) = \left[\mathbf{B}^* - \Delta t \mathbf{J}_\Delta^*\left(\frac{\vec{c}(t) + \vec{c}^{(pred)}(t)}{2}\right)\right]^{-1}$$

$$\left[\mathbf{B}^* + \Delta t \mathbf{J}^*\left(\frac{\vec{c}(t) + \vec{c}^{(pred)}(t)}{2}\right)\right]\vec{c}(t) \quad (19)$$

in which first a concentration vector $\vec{c}^{(pred)}$ is calculated for the time $t + \Delta t$. In a second step, this $\vec{c}^{(pred)}$ predicted at $t + \Delta t$ is averaged with the concentration $\vec{c}(t)$ and taken as a basis for the calculation of the fluxes. This approximates the average fluxes during the time step Δt. It should be noted that in this treatment of the nonlinearity in Eq. 19, the accuracy of the concentration-dependent flux term is enhanced by the fact that in the moving frame of reference the concentration changes in each compartment will remain small.

RESULTS

Moving grid solutions of the Lamm equation

Fig. 2 shows the results of simulations with the moving grid approach (Eq. 13, using the maximal time steps according to
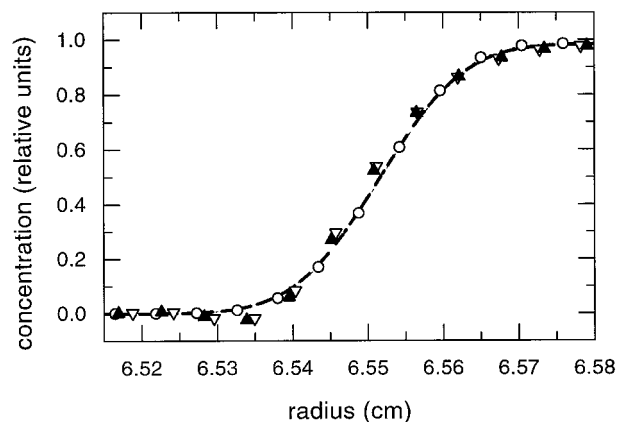

FIGURE 2   Calculated sedimentation profiles for different discretizations and computation methods under fast transport conditions ($\omega = 60,000$ rpm, $s = 10$ S, $D = 2 \times 10^{-7}$ cm^2/s). Shown are the calculated profiles at $t = 200$ s, for a solution column from 6.5 cm to 7.2 cm, with uniform initial distribution $c(r, 0) = 1$. Lines show results with a very fine grid and small time steps ($N = 10,000$, $\Delta t = 0.26$ s). Both the moving hat approach of Eq. 13 ($\cdots$), and the analog equation based on the Claverie approach in the Crank-Nicholson scheme (− −) converge (maximum difference $\leq 10^{-5}$). Symbols show results from a very coarse discretization ($N = 125$, $\Delta t = 20.9$ s) in the Claverie approach (▲), and in the approach of Eq. 13 using a stationary grid (▽) and Eq. 13 using a moving grid $s = s_G$ (○).

Eq. 6) and the correspondent Claverie approach in a Crank-Nicholson scheme (Claverie et al., 1975; Schuck et al., 1998). For very fine grids and small time steps, both methods lead to virtually the same profiles ($\Delta c \ll c_0 \times 10^{-5}$ for $N > 10{,}000$). However, for a coarse grid and large time steps, the Claverie approach (as well as Eq. 13 at a stationary grid $s_G = 0$) can lead to significant errors; in cases of high transport fluxes, even negative concentrations and oscillations near the sedimentation boundary are found. However, application of the moving grid with $s_G = s$ leads to more stable results, and converges much more rapidly toward the fine grid results (Fig. 2). With a decreasing number of compartments N, both approaches can lead to oscillations in the regions close to both ends of the solution columns, but they decay very rapidly with increasing distance from the meniscus and bottom, respectively.

The precision of the results was first tested for a noninteracting solute at different rotor speeds, sedimentation, and diffusion coefficients. In calculations using similar discretization, the moving and the stationary grid results were comparable at low ratio of transport to diffusional flux ($\omega^2 s/D < 500$ rpm^{2}s^2/cm^2), for larger ratios $\omega^2 s/D$, the moving grid did lead to an increase in precision by a factor of ~5. Correspondingly, the same precision was achieved by the moving grid method by a factor 2 fewer grid points than in the Claverie method. For example, with a moving grid using Eq. 13 and Eq. 6, a division of a 7-mm solution column into $N = 500$–1000 grid points, and for $\Delta t_{swap} < 200$ s, the maximum error was $\ll c_0 \times 0.001$ and the rms error was $\ll c_0 \times 0.0001$, independently of rotor speed, s, and D. This numerical error is below the experimental error of data acquisition in a centrifuge experiment.

Calculations for self-associating solutes were implemented for monomer-dimer and monomer-trimer associations and tested in several ways. First, they obeyed mass balance and approached the correct sedimentation equilibrium distributions, as analyzed by independent conventional sedimentation equilibrium methods. Second, in the limit of very small or very large association constants, respectively, the calculated distributions converge correctly to those of a single noninteracting monomer or oligomer, respectively. Third, independent calculations both with a static equidistant grid, as described in Claverie et al., 1975, and with a moving grid, converge with finer discretization in space and time toward the same profiles, which have been shown by Claverie (1976) to represent the correct sedimentation distributions. For large self-associating solutes at high rotor speeds, the gain in precision by the moving grid method was found to be approximately a factor of 10.

Noninteracting and homogeneous associating systems are similar in that they both allow the use of experimental scans at an early time of an experiment as initial condition for the solution of the Lamm equation. This option has been implemented as described in Schuck et al., 1998. It can avoid initial experimental imperfections that can be introduced, for example, by the finite time needed for acceleration of the rotor, or by the use of artificial layering techniques (Cox, 1966).

Global analysis of low-speed and high-speed experiments for a single noninteracting solute

Data analysis with numerical solutions of the Lamm equation allows for the extraction of sedimentation coefficients from the approach to equilibrium in conventional short-column low-speed sedimentation equilibrium experiments (Demeler and Saber, 1998; Schuck et al., 1998). Since this method can take into account the end effects of the solution column, it also allows investigators to perform short-column high-speed sedimentation velocity experiments. Fig. 3 shows low-speed and high-speed sedimentation profiles, respectively, simulating the experimental configuration of a sedimentation equilibrium experiment, followed by shaking of the cell allowing for redistribution of the protein, and a rapid high-speed sedimentation.

The data were analyzed using the Lamm equation, and treating the loading concentration and a small baseline offset as unknown variables. From both parts of the exper-
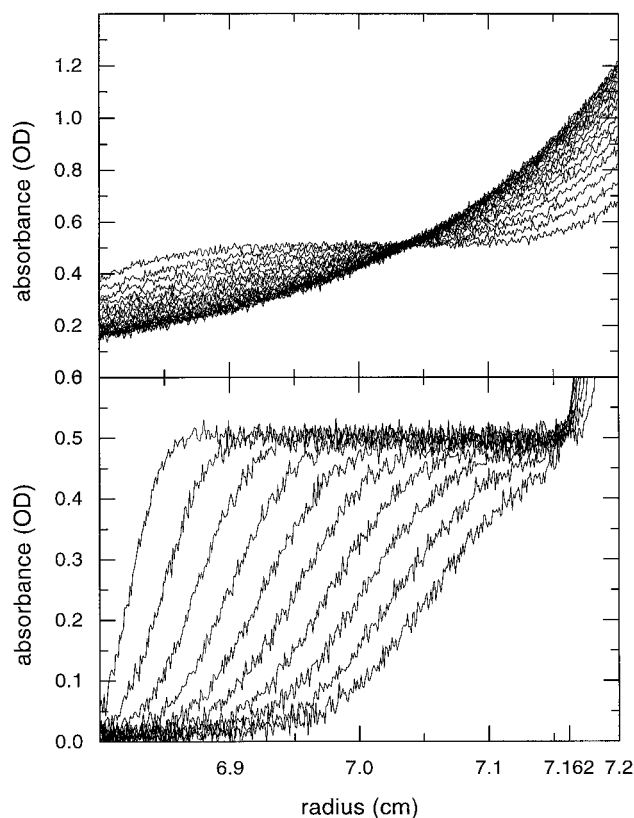

FIGURE 3 Calculated sedimentation profiles of a protein with $M = 100$ kDa (at a partial specific volume of 0.73 cm^3/g) and $s = 7$ S. Simulations were performed for a 4-mm solution column at a rotor speed of 8000 rpm, with distributions recorded at time intervals of 3600 s and radial increments of 0.001 cm (*upper panel*); and for a 4-mm column at 40,000 rpm with distributions at time intervals of 300 s (*lower panel*). The initial absorbance was 0.5 OD, and Gaussian distributed noise of 0.01 OD and a baseline offset δ of 0.01 OD were added.

iment, the diffusion coefficient D (or the buoyant molar mass) as well as the sedimentation coefficient s can be obtained. This is demonstrated in Fig. 4 A, which shows the one-standard-deviation contour maps of the error surfaces of the nonlinear regression, expressed in s and M as independent parameters. As can be expected, the low-speed experiment gives relative precise information on M, while yielding only moderate accuracy for s. At a higher rotor speed, this contour map changes its shape toward a very well-defined s, but with a relative high uncertainty in M. This situation remains virtually unchanged for larger column heights and a correspondingly larger amount of data, as indicated by the contour of a 10-mm column height experiment shown in Fig. 4 A.

High statistical accuracy simultaneously in s and M can be achieved in a global fit to both low- and high-speed
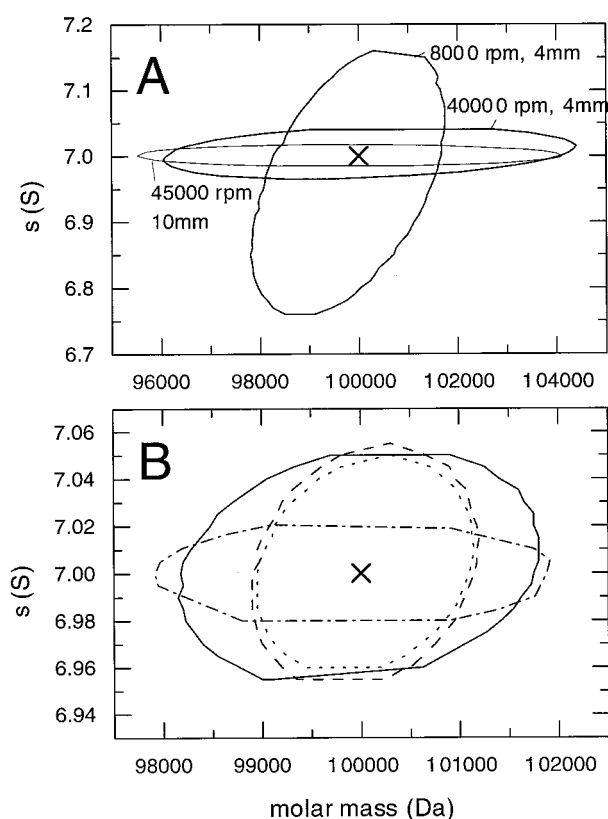

FIGURE 4 Statistical analysis of the short-column concentration profiles shown in Fig. 3 and of calculated sedimentation profiles for the same solute ($\times$), in a 10-mm long-column experiment at 45,000 rpm with distributions recorded in 500-s intervals (data not shown). (A) One-standard-deviation contour maps of the error surface for the independent analysis of each data set. Data analysis was based on F-statistics (Bevington and Robinson, 1992), treating δ and a_0 as unknown, floating parameters. Data points in the steep part of the high-speed sedimentation profiles near the bottom ($r >$ 7.162 cm) were excluded from the analysis. (B) Results of global analyses of the short-column data shown in A and B, with baseline and initial absorbance treated as independent parameters in sets A and B (—), constraining the baseline to be identical while using independent initial absorbancies (– –), and constraining both the baseline and initial absorbance to be identical ($\cdots$). Global analysis of the 10-mm column at 45,000 rpm, and the 4-mm at 8000 rpm, using independent baseline offsets and loading absorbancies (– $\cdot$ –).

short-column data sets, as demonstrated by the corresponding contour maps of the error surface in Fig. 4 B. The accuracy can be further increased if the baseline offset and/or the loading concentration can be assumed equal in both parts of the experiment. This can be fulfilled experimentally if the buffer absorption remains constant and if the protein does not pellet or absorb to the cell walls during the first equilibrium experiment. For the global analysis of a long-column high-speed and a short-column low-speed experiment, it may not be possible to assume the loading concentration and the baseline offset to be identical. Compared to the global short-column analysis, this results in higher precision in s, but lower precision in M.

Global analysis for a solute in monomer-dimer self-association

To simplify the treatment of self-associating systems, it was assumed that no volume change occurs during association. This allows the application of the Svedberg equation (Svedberg and Pedersen, 1940) to relate the diffusion coefficients of monomer and dimer, and to map the parameter space in the data analysis from (s_1, s_2, D_1, D_2) to (M_1, s_1, s_2). Sedimentation profiles were calculated for a solute of monomer molar mass 100,000 Da and $s_1 = 6.5$ S, dimerizing with an equilibrium constant $K_2 = 3.98$/OD [$\log_{10}(K_2) = 0.6$] to a component with a molar mass of 200,000 Da and $s_2 = 10$ S, at a loading absorbance of $a_0 = 0.5$ OD and 0.01 OD Gaussian distributed noise.

First, in order to study the ability to identify the presence of a monomer-dimer equilibrium, we analyzed the simulated data with an impostor single noninteracting species model. Using a 4 mm column at 8000 rpm, statistically acceptable fits could be achieved for a single species of $M = 164300$ Da and $s = 8.84$ S (rms deviation 0.010014). For high-speed experiments, high deviations were found only in the steepest gradient near the bottom of the column. Excluding the outer 0.5 mm of the solution column, which can be necessary in practice due to optical artifacts in the vicinity of the cell bottom, reasonable fits could be achieved with $M = 97600$ Da and $s = 8.29$ S (rms deviation 0.01097). Remarkably, the ability to fit the monomer-dimer equilibrium data with a single species model using these parameters was found to be qualitatively independent of the length of the solution column. It should also be noted that the broadening of the sedimentation boundary caused by the heterogeneity of the association state closely resembles diffusional broadening of a solute smaller than the monomer. In contrast, global analysis of short-column experiments at different speeds (4 mm, 8000 rpm and 45,000 rpm, similar to those shown in Fig. 3) did not allow satisfactory modeling of the data with the impostor model (best-fit $M =$ 163,160, $s = 8.33$ S, rmsd $= 0.01266$).

For the case of the correct application of a monomer-dimer model with known monomer buoyant molar mass (e.g., from known amino acid composition), the contour

maps corresponding to the confidence level of one standard deviation together with the statistical accuracy of the equilibrium constant are shown in Fig. 5. As can be expected, the short-column low-speed data have much more information on the equilibrium constant ($\log_{10}(K_2) \in [0.52, 0.66]$), while the sedimentation coefficients are highly correlated and little information can be obtained (Fig. 5 A). The high-speed experiment at the same column height of 4 mm offers improved, but still poor, accuracy of the sedimenta-

tion coefficients, while containing very little information on the equilibrium constant ($\log_{10}(K_2) \in [0.35, 0.91]$). The use of an increased column height of 10 mm, which leads to a considerably increased data base, improves the precision of the sedimentation coefficients ($s_1 \in [6.0, 6.9]$, $s_2 \in [9.84, 10.26]$), but still does not lead to satisfactory precision of the association constant ($\log_{10}(K_2) \in [0.40, 0.75]$) (Fig. 5 A).

Therefore, global analysis procedures were applied to different configurations. The highest accuracy in the sedimentation coefficients was achieved in the combined analysis of two high-speed experiments with 7-mm columns and loading concentrations at a ratio 10:1 (simulated by $a_0 = 1$, and $a_0 = 0.5$ at a second wavelength with fivefold higher solute extinction). This resulted in sedimentation coefficient estimates with relative errors of only 1.2% and 1% for the monomer and dimer, respectively, and an estimate for the association constant of $\log_{10}(K_2) \in [0.535, 0.678]$ (Fig. 5 B). The highest accuracy in the equilibrium constant was achieved by the global analysis of both low- and high-speed short-column experiments in the configuration similar to that of Fig. 3. Assuming the loading concentration and/or the unknown baseline offset to be identical for each part of the experiment, an association constant $\log_{10}(K_2) \in [0.565, 0.632]$ and relative errors of the monomer and dimer sedimentation coefficients of 5% and 3%, respectively, were obtained. The extension of the solution column in the high-speed experiment introduces an increased number of data points. However, since the baseline offset and the initial absorbance in the different solution columns may not necessarily be identical, this configuration did lead to only slightly improved precision of the sedimentation coefficients, and to a less precise estimate of the equilibrium constant ($\log_{10}(K_2) \in [0.545, 0.651]$).

DISCUSSION

The applicability and the advantages of using direct fitting of the Lamm equation to analytical ultracentrifuge data for the analysis of hydrodynamic shapes and gross conformation of solutes has been demonstrated in different laboratories (Demeler and Saber, 1998; MacPhee et al., 1997; Schuck et al., 1998; Schuck and Millar, 1998; Stafford, 1998). Among its virtues is the ability to describe the boundary effects at the end of the solution column, which allows the study of small solutes with high diffusion coefficient or, complementary to that, it allows for the use of smaller sample volumes and lower rotor speeds in studies of large solutes. In addition, due to the lack of analytical solutions describing the sedimentation of systems of interacting solutes, only numerical integration of the Lamm equations has the potential to rigorously obtain information on hydrodynamic shapes of reversibly formed protein complexes from analytical ultracentrifugation experiments. This method could provide insights into the gross conformation of complexes, and consequently provide insight to some extent into the mechanism of interaction for a large class of protein-protein and protein-DNA systems.
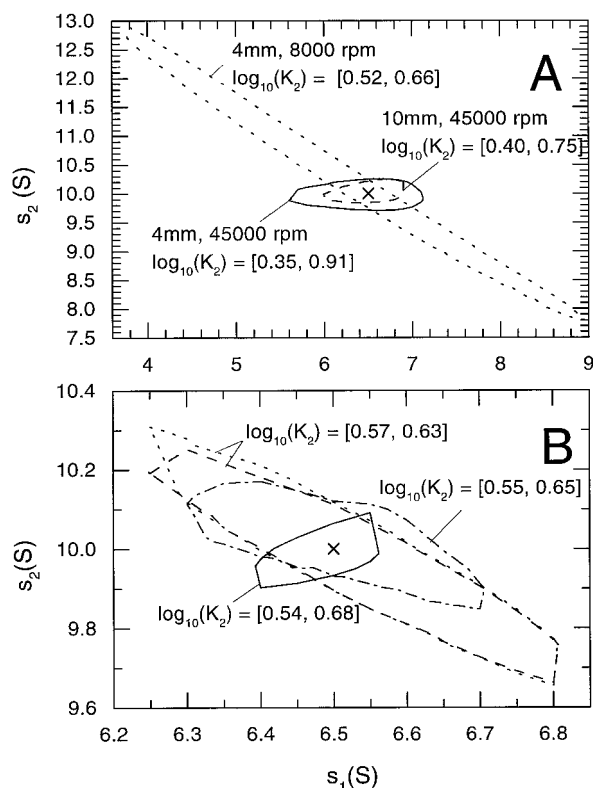
FIGURE 5 One-standard-deviation contour maps of the error surface in the analysis of a monomer-dimer self-association. Data were generated using $M = 100$ kDa (at a partial specific volume of 0.73 cm³/g), monomer $s_1 = 6.5$ S and dimer $s_2 = 10$ S ($\times$), with an association constant $K_2 = 3.98/\text{OD}[\log_{10}(K_2) = 0.6]$. Data analysis was based on F-statistics, treating association constant K_A, baseline offset δ, and loading absorbance a_0 as unknown, floating parameters. Separately calculated confidence intervals of the equilibrium constant K_A (using the sedimentation coefficients as floating parameters) as indicated for each experimental configuration. Radial data increments were 0.001 cm. Unless noted otherwise an initial absorbance $a_0 = 0.5$ OD was used, and Gaussian distributed noise of 0.01 OD and a baseline offset δ of 0.01 OD were added. Data points in the steep part of the high-speed sedimentation profiles near the bottom were excluded from the analysis. (A) Independent analyses: solution column of 4 mm at a rotor speed of 8000 rpm, with distributions recorded at time intervals of 3600 s ($\cdots$), 4-mm column at 45,000 rpm recorded at time intervals of 300 s (——), and 10-mm column at 45,000 rpm at time intervals of 300 s (— —). (B) Global analyses: two 7-mm columns at 45,000 rpm with a ratio of loading concentrations of 10:1, achieved by loading absorbancies $a_0 = 1$ and $a_0 = 0.5$ at wavelengths with fivefold different solute extinction (such as $\epsilon_{280}/\epsilon_{230}$) (——); one 4-mm column at rotor speeds of 8000 rpm and 45,000 rpm, constraining δ and a_0 to be identical in each set (— —), or constraining δ to be identical and independently floating a_0 in each set ($\cdots$); a 4-mm column at 8000 rpm combined with a 10-mm column at 45,000 rpm, with independently floating δ and a_0 (— $\cdot$ —).

To achieve this goal, two major current difficulties have to be resolved. First, the computational cost of the analytical approach in most cases still seems to be prohibitive, despite considerably increased computational capacities. This difficulty increases with higher sedimentation fluxes and lower diffusional fluxes, or with increasing size of the solutes and increasing rotor speed, respectively. In the present paper we have addressed this problem by combining the most commonly used numerical strategy devised by Claverie (Claverie, 1976; Claverie et al., 1975) with a moving grid technique. In contrast to other moving or adaptive grid approaches (Cox and Dale, 1981; Dishon et al., 1966; Cann and Kegeles, 1974), the exponential spacing and movement of the grid points in Eqs. 4 and 5 has the unique properties of constantly traveling with the solute while mapping onto itself after certain time intervals. Transformations of the radial variable similar to Eq. 4 have proven extremely useful in the derivation of approximate analytical solutions to the Lamm equation for ideal noninteracting solutes (Faxén, 1929; Fujita and MacCosham, 1959; Fujita, 1962; Holladay, 1979a), their subsequent application to nonlinear regression of sedimentation velocity data (Philo, 1997; Behlke and Ristau, 1997; Holladay, 1979b, 1980), and to the time-derivative analysis in the determination of $g^*(s)$ (Stafford, 1992). The introduction of this transformation into the numerical finite element solution provides a frame of reference in which, for ideal noninteracting solutes, sedimentation is virtually absent, and the Lamm equation essentially reduces to a diffusion equation that is easier to solve. The corresponding gain in accuracy is demonstrated in Fig. 2, which shows how a very small number of moving grid points can describe a sedimentation boundary comparatively well. For interacting solutes, although the movement of the grid does not match that of all components, the sedimentation fluxes are still greatly reduced. This can substantially diminish the magnitude of the nonlinear terms of the Lamm equation that are introduced by chemical reactions among solutes and, in turn, improve the accuracy and efficiency of the numerical solutions.

As pointed out by Demeler and Saber (1998), instabilities can occur at the end of the solution column using the Claverie approach. This problem was found in a similar magnitude in the Claverie approach and with the moving grid approach presented here. Consistent with the findings of Demeler and Saber, these oscillations rapidly decay with increasing grid size and distance from the bottom of the solution column, and in practice remain well within the range of the well-known artifacts of the optical detection system of the analytical ultracentrifuge.

The second major difficulty in sedimentation studies of reversibly interacting solutes is their high number of unknown hydrodynamic parameters in addition to unknown binding constants. In particular, in contrast to heterogeneous interactions (Stafford, 1998), for self-associating solutes no independent measurement of the sedimentation coefficient of the species can be performed. Key to this problem could be the use of a large experimental database from different

experiments and their global analysis (Beechem, 1992; Stafford, 1998). While traditional analytical ultracentrifuge experiments already allow a broad variety of experimental configurations (for example, with different loading concentrations, rotor speeds, and column heights), even more configurations are possible by the use of direct Lamm equation fitting. These include approach to equilibrium analysis in low-speed sedimentation equilibrium experiments, and short-column high-speed sedimentation velocity experiments that do not exhibit clear solvent and solution plateaus. Since it is not obvious how to utilize such experiments for rigorous hydrodynamic shape analysis of reversibly formed protein complexes, we have investigated their information content by analyzing their respective error surfaces for simulated noisy ultracentrifuge data.

As can be seen in the contour maps of Figs. 4 and 5, the information content strongly depends on the centrifugal fields used in the experiments. This is in accordance with common experimental experience and relates to differences in the conditioning of analyses of a translatory movement of a boundary, diffusional boundary spreading, and exponential equilibrium analysis, which, to a rotor-speed dependent degree, govern the analysis. It is noteworthy that for a noninteracting solute in high-speed sedimentation velocity experiments the sedimentation coefficient confidence limits are very narrowly confined, while only poor estimates of the diffusion coefficient seem possible. This was found to be qualitatively independent of the column length, indicating that analysis of the boundary spreading during the relative short duration of a high-speed experiment is an ill-conditioned problem.

Precise parameter estimates were obtained with a global analysis of an approach to equilibrium experiment and a short-column high-speed experiment. This combines the strength of an equilibrium analysis, which is its independence of hydrodynamic parameters, with the strength of sedimentation velocity studies; i.e., the ability to very precisely measure the translation of the boundary. In practice, this sequence of experiments would only slightly differ from the commonly used sequence of a conventional sedimentation experiment followed by a final overspeeding phase intended for the measurement of the background absorption offset. The only additional requirements would be scanning of the transient states in both parts and mixing of the solution in between. The advantage over separate traditional equilibrium and long-column sedimentation velocity experiments is the considerably smaller amount of sample needed by using only one single short column and the identical baseline offsets and loading concentrations. Also, it is noteworthy that a final high-speed phase following sedimentation equilibrium experiments can substantially improve the ability to identify the presence of self-association.

Interacting systems provide a much more complicated problem, but as demonstrated for the case of monomer-dimer self-association, the same principles lead to the most informative experimental configuration. It was found that the high-speed data alone can only poorly measure the

association constant, while also giving only modestly precise estimates of the sedimentation coefficients (Fig. 5 *A*). Conceptually, this can be understood by considering the Lamm equation analysis a transformation of the sedimentation data into a binding isotherm $s_w(c)$. It is well known that the reliable analysis of a binding isotherm requires the data to span two orders of magnitude in concentration, which can be difficult to achieve in the absorption optical system of the analytical ultracentrifuge at the given linear range and experimental noise. This uncertainty of the association constant in turn affects the precision of the monomer and dimer sedimentation coefficients, respectively. Low-speed data alone have information on the equilibrium constant, but virtually none on the sedimentation coefficients. Therefore, global analysis seems to be essential in treating and identifying interacting systems. As suggested by the error contours in Fig. 5 *B*, the determination of the equilibrium constant using the short-column approach to equilibrium technique again can be combined with the hydrodynamic information of the high-speed data set. The error analysis also indicates that, in an alternative configuration, the global analysis of different long-column high-speed experiments would require the use of considerably different loading concentrations, which may be achieved, for example, by exploiting multi-wavelength techniques.

In summary, we have presented a numerical method and have explored experimental strategies for the efficient quantitative sedimentation analysis for ideal noninteracting and self-associating systems. Previous methods for this problem include the study of the concentration dependence of the second moment of a sedimentation boundary (Adams, 1992), and the qualitative analysis of the boundary shape assuming vanishing diffusion in Gilbert theory (Gilbert, 1955). The presented approach is more general in that it allows the complete use of several series of concentration distributions in different centrifugal fields in a global quantitative analysis. While the data simulation was based on the use of an absorbance optical system, the approach can be incorporated in the time-derivative analysis of interference optical ultracentrifuge data that can provide enhanced sensitivity (Stafford, 1994). The described numerical and experimental strategies could also prove useful in the sedimentation analysis of heterogeneous interactions.

APPENDIX

In the following, the results of integration over the elements and their derivatives are given. The products $P_k P_j$ are non-zero only for neighboring elements with $j = k - 1$, k, or $k + 1$, and consequently the integrals can be expressed as tridiagonal matrices of simple polynomials. They have to be calculated only once using the initial grid $r_{k,0}$, since the propagation of the grid according to Eq. 4 leads to a uniform stretching that can be accounted for separately in Eq. 12.

In accordance with the terminology introduced by Claverie et al. (1975) and the integrals tabulated by Cox and Dale (1981) for the special case of an equidistant grid, the integrals of the elements $\mathbf{B}_{kj} = \int_m^b P_j P_k r\,dr$ give

$$\mathbf{B}_{k,k-1} = \mathbf{B}_{k-1,k} = (r_k^2 - r_{k-1}^2)/12$$

$$\mathbf{B}_{k,k} = (r_{k+1} - r_{k-1})(r_{k-1} + 2r_k + r_{k+1})/12$$

$$\mathbf{B}_{1,1} = (2mr_2 - 3m^2 + r_2^2)/12$$

$$\mathbf{B}_{N,N} = (3b^2 - 2br_{N-1} - r_{N-1}^2)/12 \qquad (A1)$$

For the integrals $\mathbf{A}_{kj}^{(1)} = \int_m^b (\partial P_j/\partial r)(\partial P_k/\partial r)r\,dr$, $\mathbf{A}_{kj}^{(2)} = \int_m^b P_j(\partial P_k/\partial r)r\,dr$, and $\mathbf{A}_{kj}^{(3)} = \int_m^b (\partial P_j/\partial t)P_k r\,dr$ governing the diffusion and sedimentation fluxes and the movement of the grid, respectively, we get

$$\mathbf{A}_{k,k-1}^{(1)} = \mathbf{A}_{k-1,k}^{(1)} = 0.5(r_k + r_{k-1})/(r_{k-1} - r_k)$$

$$\mathbf{A}_{k,k}^{(1)} = r_k(r_{k+1} - r_{k-1})/\{(r_k - r_{k-1})(r_{k+1} - r_k)\}$$

$$\mathbf{A}_{1,1}^{(1)} = 0.5(r_2 + m)/(r_2 - m)$$

$$\mathbf{A}_{N,N}^{(1)} = 0.5(b + r_{N-1})/(b - r_{N-1}) \qquad (A2)$$

$$\mathbf{A}_{k,k-1}^{(2)} = (r_k^2 + 2r_k r_{k-1} + 3r_{k-1}^2)/12$$

$$\mathbf{A}_{k,k}^{(2)} = (r_{k-1} - r_{k+1})(r_{k-1} + 2r_k + r_{k+1})/12$$

$$\mathbf{A}_{k,k+1}^{(2)} = (-r_k^2 - 2r_k r_{k+1} - 3r_{k+1}^2)/12$$

$$\mathbf{A}_{1,1}^{(2)} = (-3m^2 - 2mr_2 - r_2^2)/12$$

$$\mathbf{A}_{N,N}^{(2)} = (3b^2 + 2br_{N-1} - r_{N-1}^2)/12 \qquad (A3)$$

$$\mathbf{A}_{k,k-1}^{(3)} = (3r_k^2 + 2r_k r_{k-1} + r_{k-1}^2)/12$$

$$\mathbf{A}_{k,k}^{(3)} = (r_{k+1} - r_{k-1})(r_{k-1} + 2r_k + r_{k+1})/12$$

$$\mathbf{A}_{k,k+1}^{(3)} = (-3r_k^2 - 2r_k r_{k+1} - r_{k+1}^2)/12$$

$$\mathbf{A}_{1,1}^{(3)} = -\mathbf{A}_{1,2}^{(3)} = r_2(m + r_2)/12$$

$$\mathbf{A}_{2,1}^{(3)} = r_2(m + 3r_2)/12$$

$$\mathbf{A}_{2,2}^{(3)} = (-mr_2 + 2r_2 r_3 + r_3^2)/12$$

$$\mathbf{A}_{N-1,N-1}^{(3)} = (br_{N-1} - 2r_{N-1}r_{N-2} - r_{N-2}^2)/12$$

$$\mathbf{A}_{N-1,N}^{(3)} = -r_{N-1}(b + 3r_{N-1})/12$$

$$\mathbf{A}_{N,N-1}^{(3)} = -\mathbf{A}_{N,N}^{(3)} = r_{N-1}(b + r_{N-1})/12 \qquad (A4)$$

Integrals of higher order, $\mathbf{U}_{kji} = \int_m^b P_i P_j (\partial P_k/\partial r)r^2\,dr$ and $\mathbf{W}_{kji} = \int_m^b P_i(\partial P_j/\partial r)(\partial P_k/\partial r)r\,dr$, occur in the Lamm equations for multi-component mixtures of interacting macromolecules, concentration dependent or radial dependent sedimentation. The nonzero integrals are

$$\mathbf{U}_{k,k-1,k-1} = (r_k^2 + 3r_k r_{k-1} + 6r_{k-1}^2)/30$$

$$\mathbf{U}_{k,k-1,k} = \mathbf{U}_{k,k,k-1} = (3r_k^2 + 4r_k r_{k-1} + 3r_{k-1}^2)/60$$

$$\mathbf{U}_{k,k,k} = (r_{k-1} - r_{k+1})(3r_k + r_{k-1} + r_{k+1})/30$$

$$\mathbf{U}_{k,k,k+1} = \mathbf{U}_{k,k+1,k} = (-3r_k^2 - 4r_k r_{k+1} - 3r_{k+1}^2)/60$$

$$\mathbf{U}_{k,k+1,k+1} = (-r_k^2 - 3r_k r_{k+1} - 6r_{k+1}^2)/30$$

$$\mathbf{U}_{1,1,1} = (-6m^2 - 3mr_2 - r_2^2)/30$$

$$\mathbf{U}_{N,N,N} = (6b^2 + 3mr_{N-1} + r_{N-1}^2)/30 \qquad (A5)$$

and

$$\mathbf{W}_{k,k-1,k-1} = -\mathbf{W}_{k,k,k-1} = (r_k + 2r_{k-1})/(-6r_k + 6r_{k-1})$$

$$\mathbf{W}_{k,k-1,k} = (2r_k + r_{k-1})/(-6r_k + 6r_{k-1})$$

$$\mathbf{W}_{k,k,k} = r_k(-r_{k-1} + r_{k+1})/[2(r_k - r_{k-1})(-r_k + r_{k+1})]$$

$$\mathbf{W}_{k,k,k+1} = -\mathbf{W}_{k,k+1,k+1} = (r_k + 2r_{k+1})/(-6r_k + 6r_{k+1})$$

$$\mathbf{W}_{k,k+1,k} = (2r_k + r_{k+1})/(6r_k - 6r_{k+1})$$

$$\mathbf{W}_{1,1,1} = -\mathbf{W}_{1,2,1} = (2m + r_2)/(-6m + 6r_2)$$

$$\mathbf{W}_{1,1,2} = -\mathbf{W}_{1,2,2} = (m + 2r_2)/(-6m + 6r_2)$$

$$\mathbf{W}_{N,N,N} = -\mathbf{W}_{N,N-1,N} = (2b + r_{N-1})/(6b - 6r_{N-1})$$

$$\mathbf{W}_{N,N,N-1} = -\mathbf{W}_{N,N-1,N-1} = (b + 2r_{N-1})/(6b - 6r_{N-1})$$

(A6)

It can be shown that they obey $\Sigma_i \mathbf{W}_{kji} = \mathbf{A}_{kj}^{(1)}$ and $\Sigma_i \mathbf{U}_{kji} = \mathbf{A}_{kj}^{(2)}$.

REFERENCES

Adams, E. T. 1992. Sedimentation coefficients of self-associating species. Analysis of monomer-dimer-*n*-mer associations and some indefinite associations. *In* Analytical Ultracentrifugation in Biochemistry and Polymer Science. S. E. Harding, A. J. Rowe, and J. C. Horton, editors. The Royal Society of Chemistry, Cambridge. 407–427.

Beechem, J. M. 1992. Global analysis of biochemical and biophysical data. *Methods Enzymol.* 210:37–54.

Behlke, J., and O. Ristau. 1997. Molecular mass determination by sedimentation velocity experiments and direct fitting of the concentration profiles. *Biophys. J.* 72:428–434.

Bethune, J. L., and G. Kegeles. 1961a. Countercurrent distribution of chemically reacting systems. I. Polymerization. *J. Phys. Chem.* 65:433–438.

Bethune, J. L., and G. Kegeles. 1961b. Countercurrent distribution of chemically reacting systems. III. Analogs of moving boundary electrophoresis and sedimentation. *J. Phys. Chem.* 65:1761–1764.

Bevington, P. R., and D. K. Robinson. 1992. Data Reduction and Error Analysis for the Physical Sciences. McGraw-Hill, New York.

Cann, J. R., and G. Kegeles. 1974. Theory of sedimentation for kinetically controlled dimerization reactions. *Biochemistry.* 13:1868–1874.

Claverie, J.-M. 1976. Sedimentation of generalized systems of interacting particles. III. Concentration-dependent sedimentation and extension to other transport methods. *Biopolymers.* 15:843–857.

Claverie, J.-M., H. Dreux, and R. Cohen. 1975. Sedimentation of generalized systems of interacting particles. I. Solution of systems of complete Lamm equations. *Biopolymers.* 14:1685–1700.

Cox, D. J. 1965. Computer simulation of sedimentation in the ultracentrifuge. II. Concentration-independent sedimentation. *Arch. Biochem. Biophys.* 112:259–266.

Cox, D. J. 1966. Sedimentation of an initially skewed boundary. *Science.* 152:359–361.

Cox, D. J. 1969. Computer simulation of sedimentation in the ultracentrifuge. IV. Velocity sedimentation of self-associating solutes. *Arch. Biochem. Biophys.* 129:106–123.

Cox, D. J., and R. S. Dale. 1981. Simulation of transport experiments for interacting systems. *In* Protein-Protein Interactions. C. Frieden and L. W. Nichol, editors. Wiley, New York.

Crank, J., and P. Nicholson. 1947. A practical method for numerical evaluation of solutions of partial differential equations of the heat-conduction type. *Proc. Cambridge Philos. Soc.* 43:50–67.

Demeler, B., and H. Saber. 1998. Determination of molecular parameters by fitting sedimentation data to finite element solutions of the Lamm equation. *Biophys. J.* 74:444–454.

Dishon, M., Weiss, G. H., and D. A. Yphantis. 1966. Numerical solutions of the Lamm equation. I. Numerical procedure. *Biopolymers.* 4:449–455.

Faxén, H. 1929. Über eine Differentialgleichung aus der physikalischen Chemie. *Ark. Mat. Astr. Fys.* 21B:1–6.

Fujita, H. 1962. Mathematical Theory of Sedimentation Analysis. Academic Press, New York.

Fujita, H., and V. J. MacCosham. 1959. Extension of sedimentation velocity theory to molecules of intermediate sizes. *J. Chem. Phys.* 30:291–298.

Gilbert, G. A. 1955. *Disc. Faraday Soc.* 20:68–71.

Gilbert, L. M., and G. A. Gilbert. 1973. Sedimentation velocity measurement of protein association. *Methods Enzymol.* 27D:273–306.

Goad, W. B., and J. R. Cann. 1969. Theory of sedimentation of interacting systems. *Ann. N.Y. Acad. Sci.* 164:172–182.

Holladay, L. A. 1979a. An approximate solution to the Lamm equation. *Biophys. Chem.* 10:187–190.

Holladay, L. A. 1979b. Molecular weights from approach-to-sedimentation equilibrium data using nonlinear regression analysis. *Biophys. Chem.* 10:183–185.

Holladay, L. A. 1980. Simultaneous rapid estimation of sedimentation coefficient and molecular weight. *Biophys. Chem.* 11:303–308.

Lamm, O. 1929. Die Differentialgleichung der Ultrazentrifugierung. *Ark. Mat. Astr. Fys.* 21B:1–4.

MacPhee, C. E., M. A. Perugini, W. H. Sawyer, and G. J. Howlett. 1997. Trifluoroethanol induces the self-association of specific amphipathic peptides. *FEBS Lett.* 416:265–268.

Marque, J. 1992. Simulation of the time course of macromolecular separations in an ultracentrifuge. II. Controlling the solute concentration. *Biophys. Chem.* 42:23–27.

Minton, A. P. 1992. Simulation of the time course of macromolecular separations in an ultracentrifuge. I. Formation of a cesium chloride density gradient at 25°C. *Biophys. Chem.* 42:13–21.

Philo, J. S. 1997. An improved function for fitting sedimentation velocity data for low-molecular-weight solutes. *Biophys. J.* 72:435–444.

Press, W. H., S. A. Teukolsky, W. T. Vetterling, and B. P. Flannery. 1992. Numerical Recipes in C. University Press, Cambridge.

Sartory, W. K., H. B. Halsall, and J. P. Breillatt. 1976. Simulation of gradient and band propagation in the centrifuge. *Biophys. Chem.* 5:107–135.

Schachman, H. K. 1959. Ultracentrifugation in Biochemistry. Academic Press, New York.

Schuck, P., C. E. MacPhee, and G. J. Howlett. 1998. Determination of sedimentation coefficients for small proteins. *Biophys. J.* 74:466–474.

Schuck, P., and D. B. Millar. 1998. Rapid determination of molar mass in modified Archibald experiments using direct fitting of the Lamm equation. *Anal. Biochem.* 259:48–53.

Stafford, W. F. 1992. Boundary analysis in sedimentation transport experiments: a procedure for obtaining sedimentation coefficient distributions using the time derivative of the concentration profile. *Anal. Biochem.* 203:1–7.

Stafford, W. F. 1994. Boundary analysis in sedimentation velocity experiments. *Methods Enzymol.* 240:478–501.

Stafford, W. F. 1998. Time difference sedimentation velocity analysis of rapidly reversible interacting systems: determination of equilibrium constants by global non-linear curve fitting procedures. *Biophys. J.* 74:301a. (Abstr.).

Svedberg, T., and K. O. Pedersen. 1940. Die Ultrazentrifuge. Theodor Steinkopff, Dresden.

Zienkiewicz, O. C., and R. L. Taylor. 1991. The Finite Element Method, 4th ed, Vol. 2. McGraw-Hill, London.